Research Article Wiley Online Library ELECTROANALYSIS

doi.org/10.1002/elan.202100628

β-Cyclodextrin PAMAM Dendrimer Surface Doped with Silver and Hexacyanoferrate (III) and its Applications for Dopamine Detection in Synthetic Samples

Priscila Fernanda Pereira Barbosa,[a] Valmor Roberto Mastelaro,[b] Eduardo Guimarães Vieira,[c] and Devaney Ribeiro do Carmo*[a]

Abstract: A synthesis of β-cyclodextrin (β-Cd) functionalized with polyamide dendrimer PAMAM G.0 complexed with silver and potassium hexacyanoferrate (III) forming a mixed-valence complex (β-Cd-PAMAM-Ag/Fe) was proposed. This material was characterized by scanning electron microscopy (SEM), infrared spectroscopy (FT-IR), X-Ray diffraction (XRD), Energy Dispersion Spectroscopy (EDS) and Electron Paramagnetic Resonance (EPR). The hybrid complex was electrochemically investigated using cyclic voltammetry and some parameters (electrolyte, concentration of electrolyte, pH and scan rate) were evaluate in order to obtain optimum analytical responses. The β-Cd-PAMAM-Ag/Fe material was successfully applied in the electrocatalytic oxidation of dopamine (DOP) using Cyclic Voltammetry (CV) and Square Wave Voltammetry (SWV).

Keywords: Cyclodextrin · Dendrimer · Silver · Hexacyanoferrate (III) · Electrochemical measurements · Dopamine

1 Introduction

Cyclodextrin (CDs) are cyclic oligosaccharides formed through starch enzymatic hydrolysis which converts starch linear chain into cyclic molecules. Their structures contain six (α-CD), seven (β-CD) and eight (ϒ-CD) D-Glucopyranose monomers linked by glycosidic bonds [1]. Groups such as hydroxylic and glycosidic oxygen atoms, make external and inner surface of CDs hydrophilic and hydrophobic, respectively [2]. The arrangement of D-Glucopyranose monomers in form of chain conformation assigns to cyclodextrins a specific truncated cone shape structure. A dynamic rearrangement of structure is possible due to rotation of D-glucose units around the glicosidic bonds, affecting CDs optical and binding properties [3]. There is a wide range for CDs applications, for example in the food industry they could limit aroma degradation and remove or deodorize undesirable components in foods, since they form inclusion complex [4]. Besides, the most desired food application is related to inclusion and release of flavours [5]. Encapsulation of bioactive compounds such as drugs for controlled release [6], excipients for pharmaceutical formulations [7] and materials for metals and organic pollutants adsorption and removal [1] are all research areas that CDs are been focus.

Formation of "inclusion complexes" is known as host-guest interaction which internal hydrophobic cavity acts as a host and substrate (molecule of interest) acts as a guest (the size must correspond to that of the host cavity). The guest is hold on within the cavity by noncovalent forces (hydrogen bonding, hydrophobic interactions, and van der Waals forces) [8]. To enhance the host-guest interaction, some chemical modifications have been reported in the literature such as formation of nanosponges, selfassemblies and the introduction of polymers or dendrimers which can be realized by several techniques [9].

Dendrimers are considered polymeric materials with an interesting, homogeneous and monodisperse architecture consisting of arms or branches which are well organized in the structure [10]. PAMAM poly(amidoamines) dendrimers are the most used and commercially available due to their properties as good compatibility, hydrophilicity, high structural flexibility and high mechanical and chemical stability [11]. At the branch end there are a great number of primary amine groups and there are other reactive groups as amide and carbonyl. The amount of these groups increases according to their generation, reaching up generation 10 [12]. The spherical geometry of PAMAM dendrimers leads to cavities inside where small molecules can be encapsulated or complexed. Besides, the high reactivity of the PAMAM surface primary amines and the lower reactivity of other functional groups, allow changes on the surface without

[a] P. F. Pereira Barbosa, D. Ribeiro do Carmo
São Paulo State University (Unesp), School of Engineering, Department of Physics and Chemistry, Campus of Ilha Solteira, 15385-000, Brazil
E-mail: devaney.carmo@unesp.br
[b] V. R. Mastelaro
Sao Carlos Institute of Physics, University of Sao Paulo, 565-905, São Carlos, SP, Brazil
[c] E. Guimarães Vieira
Department of Fundamental Chemistry, Institute of Chemistry, University of São Paulo, 05508-000 São Paulo-SP, Brazil

Supporting information for this article is available on the WWW under https://doi.org/10.1002/elan.202100628

changing the interior. In this way PAMAM dendrimers can act as an excellent platform for building new materials.

Some approaches have been made to interact cyclodextrins and PAMAM dendrimer to provide a new material from the combination of two types of molecular cavities enhancing physical and chemical properties (sorption capacity, solubility, thermal stability), for example Li et al. 2012 [13] prepared a copolymer formed between these two molecules in order to study sorption of chlorophenols from aqueous solution. Results showed that the hybrid new material exhibited high sorption amount and acceptable sorption equilibrium time toward organic compound. Roessler et al. 2001 [14] added β-cyclodextrin (β-CD) into a formulation of PAMAM/DNA and it was observed that it affected physical and chemical properties of the complexes resulting in smaller particles and more evenly distributed on the surface of the solid support favouring in situ transfection. Saraswathy et al. 2015 [15] synthesized multifunctional drug carriers using PAMAM, (β-CD) and poly(ethylene glycol) for cancer therapy target. High encapsulation capacity for hydrophobic drugs and desirable characteristics as promising drug carriers were observed for the conjugated material.

As above discussed, the hybrid material formed by PAMAM and cyclodextrin offers many advantages, can be used for several purposes and can be synthesized by different routes. However, in electrochemical field, there is a disadvantage associated to unsuitable conductivity of the material for detecting specific molecules in some potential. In order to overcome this difficult, the conductivity can be improved through incorporation of conducting materials such as metals into the hybrid material structure. In this way, silver have attracted much attention due to its quantum characteristics and large specific surface area of small diameter [16] which can be attached into the structure. Here we propose a formation of a hybrid material formed by β-CD/PAMAM G.0 (generation 0) acting as a platform for silver ions, followed by a subsequent reaction with potassium hexacyanoferrate (III).

Dopamine (DOP) is one of the most important excitatory chemical catecholamine neurotransmitters present in the brain to lead transmission from one nerve cell (neuron) to another, regulation emotion, cognition, action and motivation [17]. For some diseases (Huntington, Parkinson and Schizophrenia) the level of DA found in human bodily fluids is elevated, thus, DA is a vital diagnostic biomarker for these diseases [18]. Several methodologies have been applied in DA quantification including spectrometry [19], high performance liquid chromatography (HPLC) [20] and electroanalytical techniques [21], but electroanalytical ones are considered the most attractive because they relatively low-cost, rapid and sensitive [22]. There are no available publications concerning this hybrid material (citrate of β-cyclodextrin functionalized with PAMAM dendrimer doped with silver and iron) used as an electrochemical sensor for DOP detection and its application in synthetic urine samples.

The idea is that β-CD/PAMAM-Ag/Fe can provide a good electron transfer between the substrate (i.e., enzyme) and the electrode. Additionally, the presence of PAMAM and β-CD, which are electron acceptors, can provide a stabilizing microenvironment around the substrate. After rigorous voltammetric studies, the hibrid material will be tested for the electrocatalytic determination of DOP.

2 Experimental

2.1 Reagents and Solutions

β-cyclodextrin, polyamidoamine dendrimer (Generation 0, 20 wt% solution in metanol), L-dopamine, graphite and potassium hexacyanoferrate (III) were purchased from Sigma-Aldrich. Citric acid, boric acid, silver nitrate ($AgNO_3$) and n-propanol and all others reagents used in this work were analytical grade (Reagen, Nuclear, Vetec, Dinâmica) and were used without further purification. All solutions were prepared using deionized water with resistivity of not higher than 18.2 MΩcm. L–Dopamine solutions were prepared immediately before use.

2.2 β-cyclodextrin Modification

3.0 g of β-cyclodextrin, 1.0 g of citric acid and 10 mL of deionized water were added to a round-bottom flask and were maintained under magnetic stirring and heating at 80 °C for 3 hours in order of enhancing β-cyclodextrin capacity to bond with other molecules. The mixture was washed exhaustively with n-propanol and vacuum filtered to remove unreacted binder and the solid was dried in a vacuum oven at 45 °C for 24 hours. Figure 1 shows the schematic representation for the formation of β-CD-cit

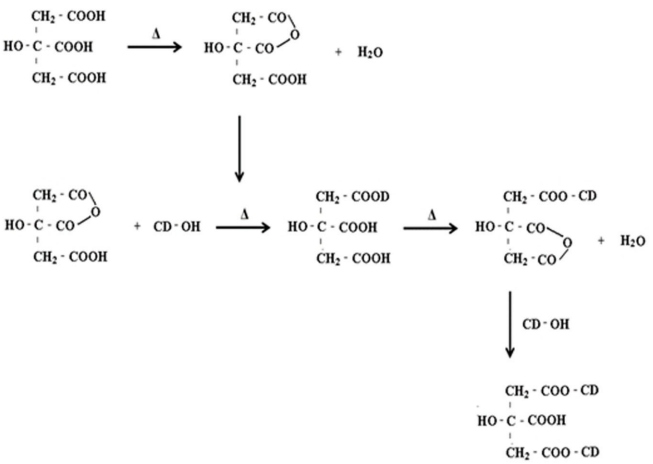

Fig. 1. Schematic representation of the formation of β-CD-cit.

2.3 Functionalization of β-cyclodextrin Citrate with Poly(Amidoamine) Dendrimer

β-cyclodextrin citrate was functionalized according to the procedure described in the literature [23], but with some modifications as shown the scheme illustrated in Figure S1 (Supplementary Information). In a 50 mL round-bottom flask, 2.21 g of β-cyclodextrin citrate, 2.23 mL of dendrimer, and 20.0 mg of acid boric (as catalyst) were dissolved in 25 mL of n-propanol. The mixture was refluxed for 48 hours at 95 °C and when the reaction was completed the solid product was vacuum filtered and washed with the solvent used. The final product was dried in a vacuum oven at 60 °C for 8 hours. The obtained material was named as β-CD-PAMAM.

2.4 Preparation of β-CD-PAMAM-Ag/Fe Hybrid Material

The formation of the hybrid material with the mixed valence complex linked in the structure was prepared following two steps. First, 500 mg of β-CD-PAMAM was dissolved in 25 mL of hydroalcoholic solution (n-propanol/deionized water) (50 % v/v) of silver nitrate (0.01 mol L^{-1}). The system was kept under stirring for 3 hours at room temperature and the solid phased was vacuum filtered and washed with water/n-propanol. The obtained material β-PAMAM-Ag was dried at 45 °C. In the second step, 250 mg of β-CD-PAMAM-Ag were added to 25 mL of potassium hexacyanoferrate (III) solution (0.01 mol L^{-1}) (water/n-propanol 50 % v/v) and kept under stirring for 3 hours. The solid phase was separated by vacuum filtration, washed with water/n-propanol and dried at 45 °C. The material was stored from the light and described as β-CD-PAMAM-Ag/Fe, which presented dark blue color.

2.5 Preparation of β-PAMAM-Ag/Fe Modified Graphite Paste Electrode

The graphite paste electrode (GPE) modified with the hybrid material was prepared by mixing 20 mg of β-CD-PAMAM-Ag/Fe with 80 mg of graphite and 20 µL of mineral oil. The mixture was homogenized and placed on tip of electrode avoiding possible air gaps.

2.6 Interference Study

The possible interference effect was investigated using SWV for the β-CD-PAMAM-Ag/Fe system in the electro-oxidation of dopamine, since some compounds such as urea (UR) and ascorbic acid (AA) are used in association with some pharmaceutical drugs or present in biological fluids (e.g., urine), it is important to evaluate the interference signal obtained. Two solutions were prepared, solution A (L-dopamine 0.01 mol L^{-1}) and solution B (UR + AA 0.01 mol L^{-1}). In the electrochemical cell (KNO_3 as electrolyte) was added 3.0×10^{-6} mol L^{-1} of solution A and in sequence aliquots of different concentrations of solution B were added (1.0×10^{-5} mol L^{-1}, 2.0×10^{-5} mol L^{-1}, 4.0×10^{-5} mol L^{-1} and 5.0×10^{-5} mol L^{-1}).

2.7 Application of the Method in Synthetic Urine Samples

As a simple and fast application, the modified electrode was used to detect/quantify DOP in synthetic urine, prepared as Laube et al. [24]. Where 2 mmol L^{-1} of citric acid, 25 mmol L^{-1} of Sodium Bicarbonate, 170 mmol L^{-1} of urea, 2.5 mmol L^{-1} of Calcium Chloride, 90 mmol L^{-1} of Sodium Chloride, 2.0 mmol L^{-1} of Magnesium Sulfate, 25 mmol L^{-1} of Ammonium Chloride, 7 mmol L^{-1} of Potassium dihydrogen phosphate and 7 mmol L^{-1} of dipotassium hydrogen phosphate were added to a 500 ml bottom flask and completed with deionized water. The solution pH was adjusted to 6 using hydrochloric acid. Quantification of DOP samples was performed in a solution of KNO_3 1.0 mol L^{-1} using spiked method. The solution was spiked by adding four aliquots of different concentrations in the KNO_3 solution containing synthetic urine. This procedure was made three times (n = 3) for square wave technique. The recovery studies allowed to evaluate the accuracy of the proposed method.

2.8 Techniques of Characterization

2.8.1 Fourier Transform Infrared Spectra (FTIR)

The vibrational spectra of β-PAMAM-Ag/Fe and its precursors were recorded at a Nicolet 5DXB FTIR spectrometer. Where 150 mg of KBr were grounded in a mortar and 15 mg of the solid sample was grounded with KBr to produce a 1 wt.% mixture, resulting in pellets. 128 scans were collected for each sample at a resolution of ±4 cm^{-1} and at the range of 4000 to 400 cm^{-1}.

2.8.2 X-ray Photoelectron Spectroscopy

The XPS analysis was performed using a Scienta Omicron ESCA spectrometer with monochromatic source of Al kα emission (1486.7 eV) and a hemispheric analyzer EA125 with passer energy adjusted to 50 eV. All XPS spectra were analyzed using the CasaXPS software, and the high-resolution spectra data were treated using the Shirley method and the remaining noises were corrected based on the C 1s energy (284.6 eV). The spectra were deconvolved using the product of the Gaussian and Lorentzian functions, while the peak areas were determined using the $Ag3d_{5/2}$ and $Ag3d_{3/2}$ standards.

2.8.3 Electron Paramagnetic Resonance Analyses (EPR)

Wave EPR data were recorded in a CW-Bruker instrument, model EMX, operating at X-band (9.4 GHz, 20 mW power, 100 kHz frequency amplitude). The magnetic field was calibrated using 2,2-diphenyl-1-picrylhydrazyl (DPPH) as standard (g = 2.0036). MATLAB 2015a pro-

grams (MathWorks) were used to adjust the simulation data by the EasySpin package [25].

2.8.4 Scanning Electron Microscopy (SEM) and Energy Dispersion Spectroscopy (EDS)

The β-PAMAM-Ag/Fe and its precursors microstructures and constituents (EDS) were obtained after coating with gold thin film in Sputter Coater Bal-Tec SCD-050. The materials morphology was examined using a Carl Zeiss EVO LS15 model scanning electron microscope. EDS spectra was obtained using a coupled apparatus to SEM and it was used to evaluate the purity of the materials and for verifying their constituents.

2.8.5 X-ray Diffraction

The X-ray diffraction patterns (XRD) were obtained using a Siemens D 5000 diffractometer with CuKα radiation λ = 1.5406 Å, submitted to 40 KV, 30 mA, 0.05○ s^{-1} and exposed to radiation from 5 up to 60○ (2θ).

2.8.6 Electrochemical Measurements

Cyclic voltammograms were performed using the Microquimica (MQP1-PGST) potentiostat. The three-electrode system used in this study consisted of a modified working electrode (graphite paste electrode), an Ag/AgCl(sat.) reference electrode, and a platinum wire as the auxiliary electrode.

3 Results and Discussion

3.1 X-ray Photoelectron Spectroscopy

The XPS spectrum of C 1s for β-CD-citrate, illustrated in Figure 2 (A), presented the main energy peaks at 284.6; 286.5 and 288.5 eV corresponding to the C–C, C–O and C=O bonds, respectively [26]. For the material β-CD-PAMAM (Figure 2 (B)) some components were observed, however with greater intensity. The peak observed at 286.3 eV is associated to C–O or may to C–N, resulted from the amine groups present in the dendrimer structure and the peak at 288.5 eV is associated to the C=O bond.

As showed in the Figure 2 (C), the XPS spectrum of O 1s for material β-CD-citrate presented the components referring to C–O and OC=O- around 532.8 and 534.1 eV, respectively, present in β-CD-citrate, but only one component in 532.8 was found in β-CD-PAMAM (Figure 2 (D)), probably due to the increase of CO groups in the composite or the decrease of available groups of β-CD-citrate, after the functionalization reaction.

The N1s XPS illustrated by Figure 2 (E), indicates that β-CD-PAMAM has been successfully synthesized. Amine groups of the dendrimer was converted into-NC=O groups (399.8 eV) due to functionalization of the free amine (NH_2) groups with carboxylic groups of β-CD-citrate (HO–C=O). A component was also observed in 401.8 eV. The central component at 401.8 eV may be related to the N–C and HN–C of dendrimer structure[27].

In β-Cd-PAMAM G.0-Ag/Fe (Figure 2 (F)), precursor components of C1s spectrum (Figure 2 (B)) were observed, where a slight increase and decrease in the intensity of C=O and C–C bonds, respectively occurred. For O 1s spectrum (Figure 2 (G)), the same components, C–O and $OC{=}O^-$ at 532.3 and 534.3 eV of β-CD-citrate were observed. Additionally, $OC{=}O^-$ was not found in β-CD-PAMAM O 1s spectrum, but when added metals to that material, this bonding site appeared again, an indicative that one metal ion may be attracted to this site weakening the bond between O and β-Cd in –(CH_2-COOCD), as proposed by Figure S1. Or the external hydroxyl group of β-Cd might lose its H and a carbonyl group could be formed, so this is a possible site that metal ions are attracted. The N 1s spectrum consists of one doublet due to spin orbit coupling, it is clear that the profile is subtly different from Figure 2 (E). The peak at 397,5 eV is assigned to N=C, probably placed on amide carbon which electron pair can be delocalized between N and O [28]. This peak suggests that a possible interacion or a bond between O and a ion metal happened, thus the electron pair is in N [29] [30]. As expected, two peaks with binding energies were observed for Fe (Figure 2 (I)), at 708.4 eV and 721.3 eV assigned to Fe $2p_{3/2}$ and Fe $2p_{1/2}$, respectively [31]. And finally, in Figure 2 (J) two components at 369.3 and 377.4 eV corresponding to the spin orbit coupling of the Ag $3d_{5/2}$ and Ag $3d_{3/2}$ were observed, respectively, which are characteristic of Ag as oxidation number zero (metallic silver) [32].

3.2 Vibrational Spectra of β-CD-PAMAM-Ag/Fe and its Precursors

The three first spectra are related to β-cyclodextrin and its modification and functionalization with PAMAM dendrimer. All spectra were recorded in the middle of infrared (4000 to 400 cm^{-1}). Figure 3 (A) shows β-cyclodextrin (β-CD) and its characteristics bands, a broadband is observed in the region of 3455 cm^{-1} attributed to O–H bond of water and stretching vibration of O–H from β-CD and at 2917 cm^{-1} there is a stretching vibration of C–H [33]. Other peaks are observed in the regions of 1643, 1081, 1057 and 1028 cm^{-1} corresponding to δ(O–H) bending vibration, ν_s(C–O–C) glucosydic stretching vibration, ν(C–C) stretching vibrations and ν(C–O) stretching vibrations, respectively, which are in accordance with those reported in the literature [34], [35]. When citrate group was added into β-CD structure (Figure 3 (B)), the same band and peaks were observed with a very slight increase and decrease of the wavenumber, for example, O–H bond appeared at 3361 cm^{-1} and it was wider, suggesting the possible formation of hydrogen bond between this group and $\nu_{ass}(COO^-)$ and $\nu_s(COO^-)$ stretching from citrate. The other peaks occurred at 1627, 1157, 1080 and 1029 cm^{-1}. A new peak was observed at 1722 cm^{-1} attributed to stretching of carbonyl group

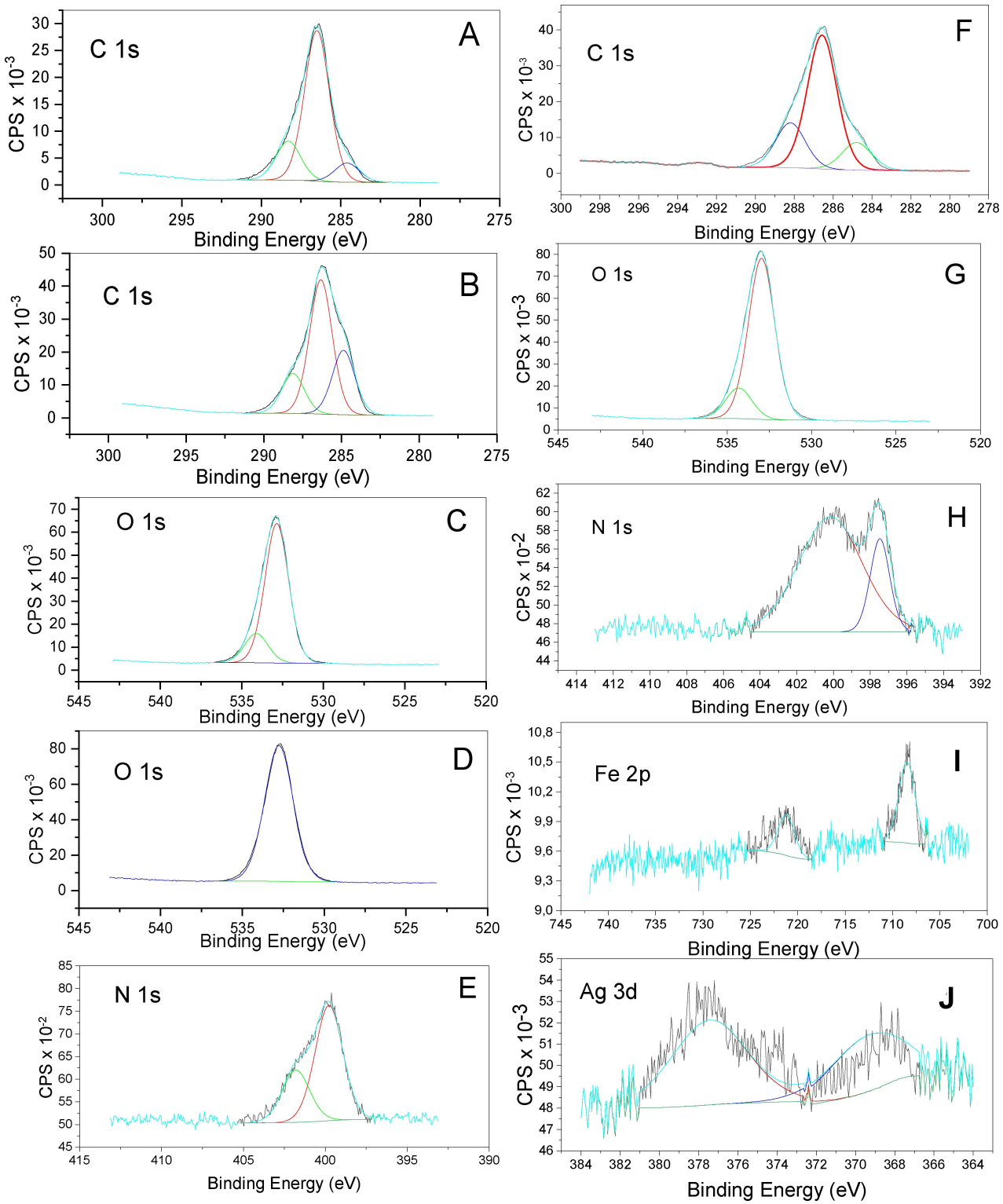

Fig. 2. XPS spectroscopy of: **(A)** C 1s β-CD-Citrate, **(B)** C 1s C 1s β-CD-PAMAM, **(C)** O 1s β-CD-Citrate, **(D)** O 1s β-CD-PAMAM, **(E)** N 1s β- CD-PAMAM and **(F)**, **(G)**, **(H)**, **(I)**, **(J)** β- CD-PAMAM-Ag/Fe of C 1s, O 1s, N 1s, Fe 2p and Ag 3d, respectively.

ν(C=O) from citric acid [36]. Besides, the intensity of the peaks attributed to ν_s(C–O–C), ν(C–C) and ν (C–O) stretching vibrations was increased. Finally, β-CD-PAMAM spectra (Figure 3 (C)) presented the characteristic peaks of modified β-CD and most changes related to interactions between β-CD and PAMAM components were observed with the appearing of two peaks at 1653 and 1573 cm^{-1} attributed to ν(C=O) and ν(N–H) stretch-

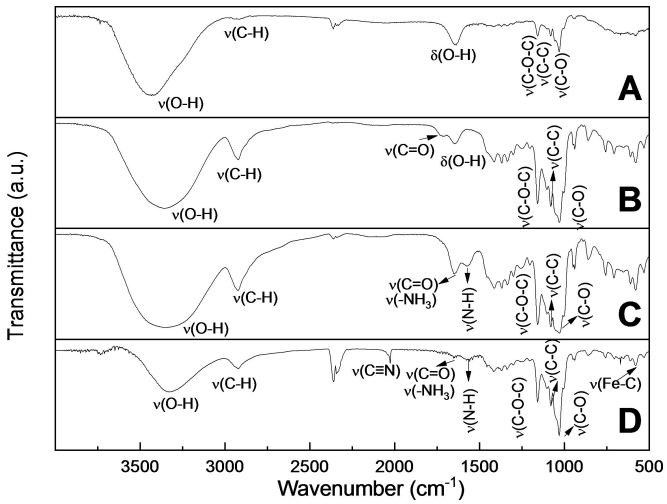

Fig. 3. Vibrational spectra of: **(A)** β-cyclodextrin, **(B)** CD-Citrate, **(C)** β-CD-PAMAM and **(D)** β-CD-PAMAM-Ag/Fe.

ing vibrations of amide groups from PAMAM structure [37].

When compared spectra of β-CD-PAMAM and β-CD-PAMAM-Ag/Fe (Figure 3 (D)) is possible to observe that peaks at 2926, 1653,1657,1158,1081 and 1028 cm^{-1} of β-CD-PAMAM-Ag/Fe are the same of its precursor with no significant displacement change, but at 2029 cm^{-1} an important vibration is observed, referring to stretching vibrations of $C\equiv N_{(\upsilon C\equiv N)}$, characteristic of potassium hexacyanoferrate (III) (HCFIII) stretching. Although the stretching vibrations $_{\upsilon C\equiv N}$ was displaced about 85 cm^{-1} to lower frequencies in relation to (HCFIII). This displacement indicates that the an intervalence complex was not been formed (Fe^{III}-CN-Ag^{I}) [38]. Furthermore, the broad band attributed to δ(O–H) bending vibration (3326 cm^{-1}) is less intense and narrower when compared to β-CD-PAMAM spectra, suggesting a possible interaction between hydrogen atoms with the intervalence complex formed and breaking of hydrogen bond of β-CD structure [36] [39].

3.3 Electron Paramagnetic Resonance (EPR)

X-band EPR spectrum for β-CD-PAMAM-Ag/Fe carried out in solid state at 77 K is shown in Figure S2. The observed spectrum displays an intense signal at $g \sim 4.3$ in the region of 160 mT. Numerous interpretations regarding g-values have been elucidated. The $g \sim 4.3$ has been assigned to both tetra- or octo-coordinated iron (III), and rhombic distortion of both tetrahedral and octahedral iron (III) [40]. Taking into account the shape of the EPR spectrum observed in Figure S2, it was assumed this peak is characteristic of high-spin ($I \pm 3/2$ and $S = 5/2$) iron (III) compounds with low symmetry as the case of β-CD-PAMAM-Ag/Fe material. In addition, the EPR measure might reveal the presence of a rhombic shape with $g_x \neq g_y \neq g_z$. Also, this typical signal has been found in several solid-state materials, metalloproteins and chelates [41].

Additionally, at low temperature (77 K) no sign of Ag can be seen by the EPR despite the ICP technique showing a concentration of 818.82 mg/Kg (ICP) however a signal related to Ag^{+} (diamagnetic) at 298 K can be seen for silver as show Figure S3. This signal suggests a strong Ag–O bond that possibly formed between OH ligands of cyclodextrin.

3.4 Scanning Electron Microscopy (SEM)

Figure S4 shows the micrographs of: β-cyclodextrin (A), citrate of β-cyclodextrin (B), β-CD-PAMAM (C) and β-CD-PAMAM-Ag/Fe (D), with a magnification of 20,000 X. β-CD and its citrate present crystal morphology with rectangular regular shapes of similar size [42] where no significant change in the microstructure can be observed between them, just the crystals (Figure S4 (B)) seem to be bigger and more organized. When β-CD is functionalized with PAMAM dendrimer (Figure S4 (C)), a reduction in particle size is observed, resulting in effective conjugation. B-CD-PAMAM-Ag/Fe (Figure S4 (D)) exhibited different sizes of irregularly blocky crystal structures, there were small particles attached to the crystals surface and this is very different from modified material without silver and iron particles, demonstrating that the interaction of these metals with the β-CD-PAMAM complex was successfully carried out.

3.5 X-ray Diffraction (XRD)

Figure 4 shows the diffractions pattern of samples. β-cyclodextrin (Figure 4 (A)) exhibited many crystalline peaks between 2 and 50° ($2\theta = 4.47$, 6.18, 8.91, 9.69, 10.22, 11.64, 12.43, 22.68, 27.02 and 31.91°) indicating that β-CD mainly existed in a crystalline form, also seen and

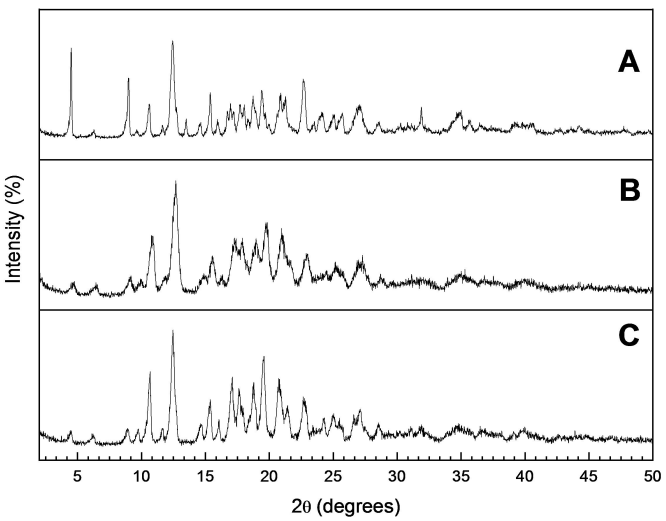

Fig. 4. XRD diffractograms of: (A) β-cyclodextrin, (B) β-CD-PAMAM and (C) β-CD-PAMAM-Ag/Fe.

described in a similar way by Trindade et al. [43]. When PAMAM is introduced into the β-CD structure (Figure 4 (B)) some changes can be observed, for example, some peaks decrease the intensity (4.47, 6.18 and 8.91°) while others increase (10.22 and 12.4°), the peak at 31,91° disappeared and from 13 to 28° the peaks seem to have higher intensity and some of them disappeared, besides reduction of the number of peaks, suggesting the formation of a material with an amorphous characteristic. The loss of crystallinity can be possibly attributed to the formation of a polymer chain β-CD and PAMAM. B-CD-PAMAM-Ag/Fe diffractogram (Figure 4 (C)) [44] also exhibited several characteristic peaks attributable to β-PAMAM, but from 13 to 28° occurs appearance of new peaks and they present higher degree of crystallinity. It can be explained by crystalline domains in silver and iron particles that were introduced.

3.6 Energy Dispersion Spectroscopy (EDS)

In Figure S5 (A), the main elements observed are carbon an oxygen being in agreement with β-CD atoms and Figure 5S (B) it was observed the same elements and nitrogen due to amines groups present in PAMAM dendrimer. For the hybrid material (Figure 5S (C) it was observed the presence of C, O, and N, characteristic of its precursor, besides the presence of Fe. It was expected the presence of Ag in this analyze but it did not occur, probably due to the region of the material that was investigated which was poor in Ag content. To overcome this situation, Ag presence was confirmed by EPR, as shown in Figure S3 and Figure S4.

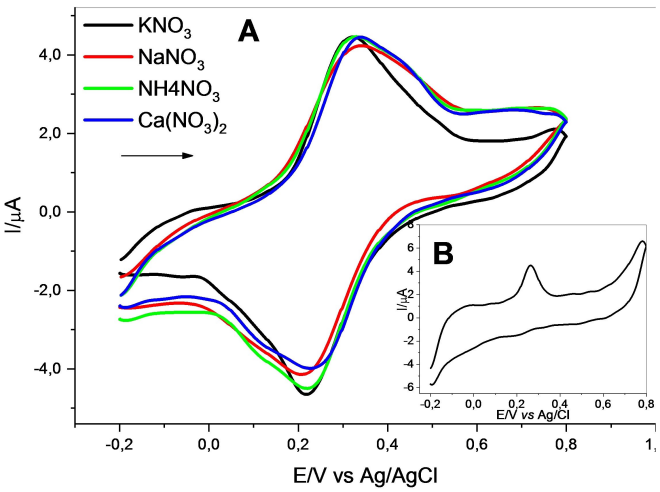

Fig. 5. **(A)** Cyclic voltammograms of the modified graphite paste with β-CD-PAMAM-Ag/Fe on different support electrolytes (20% *w/w*; $v = 20\ mV\ s^{-1}$; $1.0\ mol\ L^{-1}$) and **(B)**: cyclic voltammogram of GPE modified with β-CD-PAMAM-Ag (KNO_3; 20% (w/w); $v = 20\ mV\ s^{-1}$; $1.0\ mol\ L^{-1}$).

3.7 Electrochemical Measurements

3.7.1 Study of Cations and Anions Effect

The first electrochemical study that was taken place was the electrolyte type study, because it is known that transition metals hexacyanoferrates have a structure with a three-dimensional cubic network that allows the inflow and outflow of alkali metals (K^+, Na^+, Li^+, NH_4^+) of crystal lattice, thus the electro-activity and selectivity dependent on the electrolyte nature used. This process can modify the voltammetric performance of the material. So, in this study was verified which ions did not significantly affect the formal potential ($E^{\theta'}$), neither the current intensity of anodic/cathodic peak, indicating that the channels of the reticulum formed are larger than the radii diameters of the hydrated cations of the electrolytes tested. The electrolyte tested were KNO_3, $NaNO_3$, NH_4NO_3, and $Ca(NO_3)_2$. Figure 5 (A) shows the cyclic voltammogram of β-CD-PAMAM-Ag/Fe on those above-mentioned electrolytes. The voltammogram exhibited a well-defined peak with formal potential ($E^{\theta'}$) of 0.27 for KNO_3 ($1.00\ mol\ L^{-1}$; $v = 20\ mV\ s^{-1}$), assigned to $Fe^{II}(CN)_6/Fe^{III}(CN)_6$ redox process.

Through Table 1, it was observed that the nature of ion did not substantially influence the formal potentials ($E^{\theta'}$) of redox pair, neither the current intensity, presenting almost the same voltammetric behavior, but for K^+ anodic and cathodic peaks showed to be more defined and Ipa/Ipc value was 1, considered the better one. It can be explained by the fact that K^+ cation has hydrated radius of (0.24 nm), as a result, it easier diffuses into the cavities of β-CD-PAMAM-Ag/Fe formed, presenting better voltammetric response. For subsequent studies, KNO_3 was chosen as supporting electrolyte. Additionally, the I_{pa}/I_{pc} ratio and ΔEp varied from ~0.87 to 1.0 V and from ~0.11 to 0.13, respectively, characterizing the

Table 1. Electrochemical parameters of graphite paste modified with β-CD-PAMAM-Ag/Fe in different supporting electrolyte (20% *w/w*; $v = 20\ mV\ s^{-1}$; $1.0\ mol\ L^{-1}$).

Electrolyte	Ipa (μA)	Ipc (μA)	(I_{pa}/I_{pc})	Epa (V)	Epc (V)	*($E^{\theta'}$) (V)	*(ΔE_p) (V)	*DHC (nm) [47]
KNO_3	3.28	3.27	1.00	0.32	0.21	0.27	0.11	0.24
$NaNO_3$	2.81	3.06	0.92	0.33	0.20	0.27	0.13	0.36
NH_4NO_3	2.75	3.15	0.87	0.33	0.22	0.28	0.11	0.24
$Ca(NO_3)_2$	3.02	3.11	0.97	0.34	0.23	0.29	0.11	0.41

* $E^{\theta'}$ (V) = $(E_{pa} + E_{pc})/2$; ΔE_p (V) = $|E_{pa} - E_{pc}|$ and *DHC = Diameter of hydrated cation.

process as *quasi*-reversible [45]. This peak (at this potential) has a contribution of Ag redox process (Figure 5 (B)), but the bimetallic complex cannot be identified because in the complex, the silver hexacyanoferrate redox couple occur at a more positive potential (~0.7–0.8 V). There was an electrostatic interaction between the reactive groups of β-CD-PAMAM and hexacyanoferrate ion (cation) $[Fe(CN)_6]^{3-}$, while silver acts as a proton possible attached to the PAMAM N site or β-CD O site. [46].

3.7.2 Influence of Supporting Electrolyte Concentration

Figure S6 (A) shows the voltammetric behavior of β-CD-PAMAM-Ag/Fe at KNO_3 concentrations of 1.0×10^{-2} mol L^{-1} to 2.0 mol L^{-1}. A linear displacement of the formal potential (E°') for positive values (0.25 to 0.28 V) was observed with increasing the concentration of supporting electrolyte. As well, the current intensity increased by increasing the concentration of the cation K^+, suggesting that the ion K^+ is involved in the redox process.

A linear relationship between formal potential (E°') and the log of K^+ concentrations is observed in Figure S6 (B). The slope of the straight line was 28 mV per decade of potassium ion concentration, indicating a *quasi* Nerstian process with the transfer of two electrons [48]. The dependence of the formal potential on the logarithm of the electrolyte concentration can be explained through charge equilibrium between the cations and β-CD-PAMAM-Ag/Fe material. The electrolyte concentration chosen for subsequent studies was, therefore, of 1.0 mol L^{-1}, due to the fact that this concentration led to parameters closer to reversibility (Ipa/Ipc = 0.98), as well as better voltammetric performance.

3.7.3 Study on the Effect of Different Hydrogen Concentrations

The effect of hydrogen ion concentration was also evaluated from pH 8 to 2. From the obtained data is possible to observe that pH did not significantly change the main parameters as the (E^{θ}') formal potential, current intensity and Ipa/Ipc relation. Just for pH 5, 4 and 3 an increase was observed in the current intensity (Figure S7) [49]. pH 7 was chosen for subsequent studies.

3.7.4 Scan Rates Influence

The electrochemical behavior of GPE modified with β-CD-PAMAM-Ag/Fe at different scan rates (20–150 mV s^{-1}) is displayed in Figure S8 (A). Through cyclic voltammograms, an increase in the anodic/cathodic peak current and a displacement of (E^{θ}') for more positive potential were observed. Increases in scan rates lead to slight increases in resistance, leading to increased ΔEp. Some peaks are appearing with increasing scan rate and they are rising to more positive potential, probably silver hexacyanoferrate was formed in some site of hybrid material, but its amount was not sufficient to suppress Fe signal.

A linear dependence between current intensity of the peak (anodic/cathodic) and the square root of the scan rate is displayed in Figure S8 (B), and this is characteristic of an electrodic process controlled by diffusion for a *quasi*-reversible system [50]. As at 20 mV s^{-1} presents a better voltammetric behavior and parameters, it was chosen to perform electro-oxidation tests.

3.8 Dopamine Electrocatalytic Oxidation

The material showed a good response in the dopamine detection, for both cyclic voltammetry and square wave techniques. DOP electrooxidation using GPE modified with β-CD-PAMAM-Ag/Fe by cyclic voltammetry is shown in Figure 6. The cyclic voltammograms of: (C) represents the graphite paste modified with the hybrid material in the absence of DOP and (D) the modified GPE in the presence of 1.0×10^{-4} mol L^{-1} of this drug. An increase in the current intensity of the anodic peak followed by a decrease in the current intensity of the cathodic peak were observed in comparation with voltammogram C. The increase in the anodic peak was of 4.18 μA (almost three times higher), considering a good response taking in account that redox couple presents low current. On the other hand, graphite paste electrode did not show any redox couple in the absence of the drug (curve A) in the potential range of −0.2 to 0.8 V and in the presence of DOP (1.0×10^{-4} mol L^{-1}) (curve B) an irreversible peak at 0,37 V attributed to dopamine oxidation process was observed. In addition, the modified GPE decreased DOP electrooxidation potential in 20 mV,

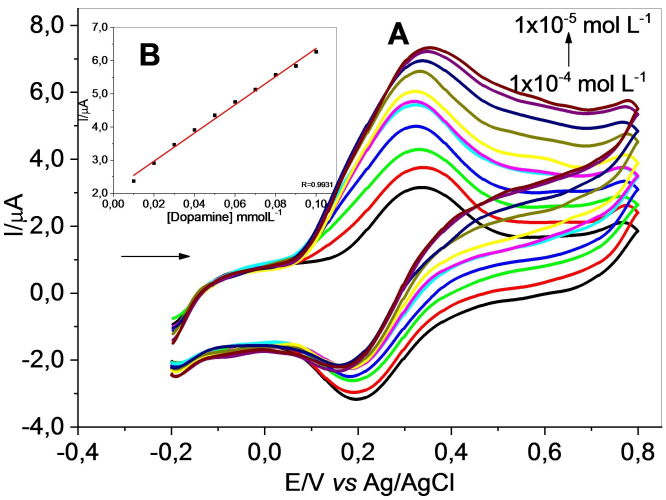

Fig. 6. **(A)** Cyclic voltammograms from GPE modified with β-CD-PAMAM-Ag/Fe in the presence of different concentrations of DOP (1.0×10^{-5} to 1.0×10^{-4} mol L^{-1}). **(B)** The analytical curve of the anodic peak for DOP detection (KNO_3; 1.0 mol L^{-1}; 20 % (w/w); pH 7.0).

probably due to an electrostatic interaction of hydroxyl group of DOP with the hybrid material surface [51].

The increase in the current intensity of the anodic peak is proportionally with the additions of DOP (increasing its concentration in the system), as illustrated in Figure 6 (A). The electrooxidation of DOP leads to formation of semiquinone as intermediate product where phenolic groups of DOP are not present in dissociate form and the amino groups is present in protonated form [52] which mechanism includes the transfer two electrons and two protons and thus radical formation is expected and at pH 7.0 this process rapidly occurs, facilitating the oxidation [53]. So, the electrochemical response is based on DOP oxidation with the metal center Fe (III) in the internal [54].

An electrochemical and a chemical processes occur as described in equation 1 and 2, respectively. The anodic scan produces Fe (III) which oxidizes DOP, in sequence, Fe (III) is reduced to Fe (II), as a result, it is electrochemically oxidized in Fe (III) again, repeating the cycle.

$$\text{EE } 2\,K_4[Fe^{II}(CN)_6] \rightleftarrows 2\,K_3[Fe^{III}(CN)_6] + 2\,K^+ + 2e^- \quad (1)$$

$$\text{EC } 2\,K_3[Fe^{III}(CN)_6] + 2X + 2\,K^+ 2 \rightleftarrows K_4[Fe^{II}(CN)_6] + Y + 2H^+ \quad (2)$$

where X = L-dopamine and Y = dopaminequinone

A linear response was achieved as DOP concentration was increased, from that an analytical curve was plotted from anodic current intensity as function of DOP concentration. The linear response (Figure 6 (B)) was found in the range of 1.0×10^{-5} to 1.0×10^{-4} mol L^{-1}, with the corresponding equation Y(μA) = 2.11 + 42.46 [Dopamine] and correlation coefficient of 0.9931. This method presented a detection limit (3SD/slope) of 7.55×10^{-6} mol L^{-1} with relative standard deviation of 3 % (n = 3) and amperometric sensitivity of 42.46 m A/mol L^{-1}.

The DOP electroanalytical oxidation in the GPE modified with the hybrid material was also carried out employing SWV as illustrated in Figure S10, where curves A and B represent the behavior of unmodified GPE in the absence and in the presence of 1.0×10^{-5} mol $L^{-1}$of DOP, respectively. The modified GPE (curve D) in the presence of 1.0×10^{-5} mol L^{-1} of DOP, showed a peak close to 0.27 V which its current increased 0.22 μA when compared with β-CD-PAMAM-Ag/Fe behavior (curve C), this increase in the current was also observed by CV. The system was made under the following conditions: KNO_3 1.0 mol L^{-1}; $f = 10$ Hz; (ω) = 50 mV. The increase in the current intensity of the anodic peak is proportionally with the additions of DOP as presented in Figure 7 (A). Figure 7(B) illustrates the analytical curve used to detect dopamine.

The analytical curve presented a linear response in the concentration range of 1.0×10^{-6} to 1.0×10^{-5} mol L^{-1} with

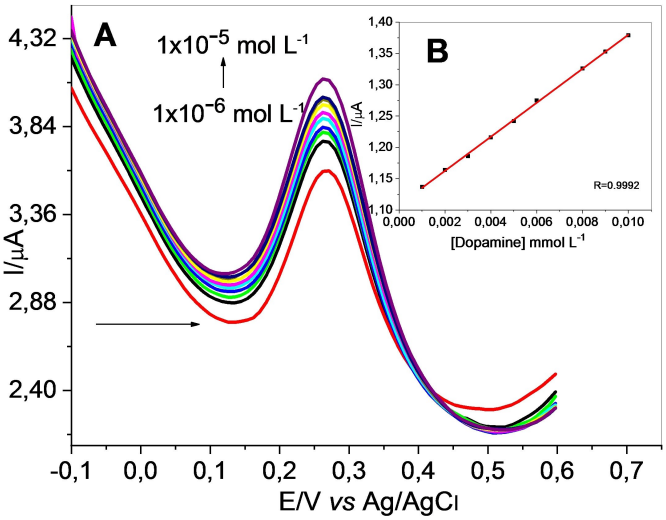

Fig. 7. **(A)** Square wave voltammograms from GPE modified with β-PAMAM-Ag/Fe in the presence of different concentrations of DOP (1.0×10^{-6} to 1.0×10^{-5} mol L^{-1}) and **(B)** The analytical curve of the anodic peak for DOP detection (KNO_3 1.0 mol L^{-1}; $f = 10$ Hz; (ω) = 50 mV).

a corresponding equation Y(μA) = 1.10 + 27.15 [Dopamine] and correlation coefficient (r^2) of 0.999. The limit of detection (3SD/slope) was $2{,}61 \times 10^{-7}$ mol L^{-1} with a relative deviation of ±1 % (n = 3) and amperometric sensitivity of 27.15 m A/mol L^{-1}.

According to the results, SWV compared to CV provided a current of highly sensitivity and better detection as demonstrated by the limit of detection and it is in agreement with other works in the literature [55]-[57]. The performance of the fabricated electrode compared with any sensor reported once is comparative or better than those cited in the literature, as demonstrated by Table 2.

Both techniques achieved good results and evidenced the sensing ability of the electrode in the presence of DOP. However, quantification of DOP encounters one problem related to the interference of several other biological molecules due their overlapping potentials, leading to poor selectivity and reusability [61], [62]. For example, interfering compounds such as urea (UR) and ascorbic acid (AA) have the same oxidation potential of DOP, influencing the reproducibility and selectivity of the electrode [63]. In this way, a study an interference study was conducted with the purpose of evaluating UR and AA current signal toward DOP electrooxidation.

3.9 Interference Study

The selectivity of the method was studied evaluating the effect of UR and AA in the current intensity of the DOP anodic peak in the modified electrode using SWV. When 3.0×10^{-6} mol L^{-1} of DOP was added in the electrochemical an increase in the current intensity was observed, but when added 4 different concentrations of UR + AA

Table 2. Comparison of this work previous reports of dopamine detection.

Electrode Material	Technique	Linear Range (mol L^{-1})	LOD[a] (mol L^{-1})	Ref.
CuHSA/GPE	DPV[c]	5.0×10^{-5} to 1.0×10^{-4}	1.70×10^{-4}	[38]
Cu-MOFs/GCE[b]	DPV[c]	5.0×10^{-6} to 1.25×10^{-4}	1.0×10^{-6}	[58]
$LaMnO_3$/GCE[b]	CV[d]	5.0×10^{-6} to 5.0×10^{-5}	6.22×10^{-6}	[59]
MoS_2 NSs/N–Gr/GPE	CV[d]	3.2×10^{-6} to 5.68×10^{-3}	1.19×10^{-5}	[60]
β-CD-PAMAM-Ag/Fe/GPE	CV[d]	1.0×10^{-5} to 2.0×10^{-4}	9.17×10^{-6}	This work
β-CD-PAMAM-Ag/Fe/GPE	SW[e]	1.0×10^{-6} to 1.0×10^{-5}	1.77×10^{-7}	This work

[a] Limit of detection; [b] Glassy Carbon Electrode; [c] Differential Pulse Voltammetry; [d] Cyclic Voltammetry; [e] SW Square Wave.

solutions no significant increase in the current was observed as illustrated in Figure 8.

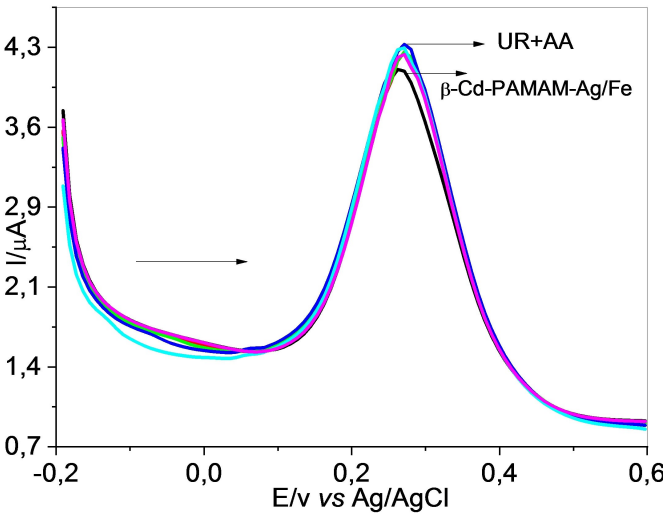

Fig. 8. Interference study of dopamine using modified GPE by SWV varying concentration of UR + AA solution (KNO_3; 1.00 mol L^{-1}; f = 10 Hz; 20 % (w/w); (ω) = 50 mV; pH = 7.0).

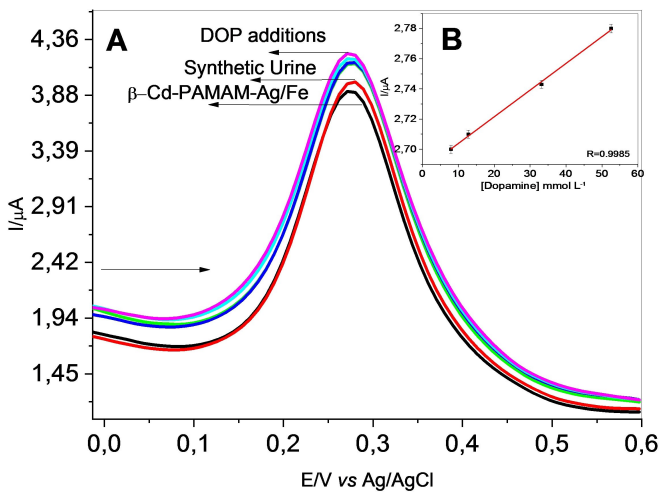

Fig. 9. Square wave voltammograms: **(A)** and calibration curve (insert) **(B)** for synthetic urine (KNO_3; 1.00 mol L^{-1}; f = 10 Hz; 20 % (w/w); (ω) = 50 mV; pH = 7.0).

Analyzing the results (Table S1), it is possible to observe that even at high concentrations, 10 times higher than DOP solution, the variation in the current intensity was less than 5 %, being an analytically permissible variation. These results confirmed that the excellent selectivity of our material towards DOP among the interferences of UR and AA. Therefore, the modified electrode can be used in the DOP detection in real samples, as synthetic urine [64]-[66].

3.10 Detection of DOP in Synthetic Samples

To verify the applicability of the proposed electrochemical sensor in practical applications using SWV, synthetic urine was prepared and reinforced with DOP (1.0×10^{-2} mol L^{-1}) and 8 μL of this solution was added in the electrochemical cell, followed by four standard additions of DOP (spiked method) (dark and light blue, green and pink lines) [67],[68]. As seen in Figure 9 (A) an increase in the current intensity was observed and an analytical curve (Figure 9 (B)) was plotted.

The recoveries data ranging from 99.22 to 100.88 % (n = 3) (Table S2) indicating the good accuracy of the method, being compatible with some recent reports in the literature [69], [70].

The use of an electrode modified graphite paste offers several advantages over other analytical techniques, such as, easy preparation, low cost, excellent limits and detection ranges and can be performed effectively several measures in short time.

4 Conclusion

To summarize, a new material was synthesized and characterized by FTIR, XRD, EPR, SEM and EDS, the results confirm that the modification really occurred (the functionalization of β-cyclodextrin with PAMAM, as expected. The hybrid material adsorbed silver, but is not complexed with hexacyanoferrate ion. The voltammetric performance was evaluated in different supporting electrolytes, in different electrolyte concentrations, pH and scan rate in order to obtain the ideal parameters for DOP detection. The voltammogram exhibited a well-defined peak with formal potential ($E_{\circ}'$) of 0.27 assigned to $Fe^{II}(CN)_6/Fe^{III}(CN)_6$ redox process. Electrooxidation of DOP was performed using CV and SW getting a linear response

in the concentration range from 1.0×10^{-5} to 1.0×10^{-4} and from 1.0×10^{-6} to 1.0×10^{-5}, respectively, resulting in detection limits of 7.55×10^{-6} mol L^{-1} for CV and 2.61×10^{-7} mol L^{-1} for SWV, being consisting with those reported in the literature. The CV and SWV studies evidenced the sensing ability and selectivity of the electrode in the presence of UR and AA, which did not show significantly interference in the current signals. Besides, the developed sensor was successfully applied for electrochemical determination of DOP in synthetic urine samples

Acknowledgements

This work was financed in part by the Coordenação de Aperfeiçoamento de Nível Superior- Brazil (CAPES) – Finance code 001. and Conselho Nacional de Desenvolvimento Científico e Tecnológico – CNPq, proc. 408104/2016-3.

Data Availability Statement

The data that support the findings of this study are available from the corresponding author upon reasonable request.

References

[1] P. F. P. Barbosa, L. R. Cumba, R. D. A. Andrade, D. R. do Carmo, *J. Polym. Environ.* **2019**, *27*, 1352–1366.
[2] S. Gao, Y. Liu, J. Jiang, Q. Ji, Y. Fu, L. Zhao, C. Li, F. Ye, *J. Mol. Liq.* **2019**, *293*, 111513.
[3] A. P. Sherje, B. R. Dravyakar, D. Kadam, M. Jadhav, *Carbohydr. Polym.* **2017**, *173*, 37–49.
[4] G. Astray, C. Gonzalez-Barreiro, J. C. Mejuto, R. Rial-Otero, J. Simal-Gándara, *Food Hydrocolloids* **2009**, *23*, 1631–1640.
[5] G. Astray, J. C. Mejuto, J. Morales, R. Rial-Otero, J. Simal-Gándara, *Food Res. Int.* **2010**, *43*, 1212–1218.
[6] R. Grillo, N. F. S. De Mello, L. F. Fraceto, C. L. Brito, G. H. G. Trossini, C. M. S. Menezes, E. I. Ferreira, C. M. Moraes, *Quim. Nova* **2008**, *31*, 290–295.
[7] T. Higashi, D. Iohara, K. Motoyama, H. Arima, *Chem. Pharm. Bull.* **2018**, *66*, 207–216.
[8] C. Gregório, *Chem. Rev.* **2014**, *114*, 10940–10975.
[9] T. A. Hagbani, T. Nazzal, *Int. J. Pharm.* **2017**, *50*, 173–180.
[10] D. R. Do Carmo, R. O. Denys, P. F. P. Barbosa, N. M. I. Godoi, *Silicon.* **2019**, *11*, 2961–2974.
[11] R. L. Zhang, B. Gao, J. Zhang, H. Z. Cui, D. W. Li, *Appl. Surf. Sci.* **2015**, *359*, 812–818.
[12] Y. Zhu, Y. Niu, H. Li, B. Ren, R. Qu, H. Chen, Y. Zhang, *Ecotoxicol. Environ. Saf.* **2018**, *162*, 253–260.
[13] N. Li, Z. Mei, X. Wei, *Chem. Eng. J.* **2012**, *192*, 138–145.
[14] B. J. Roessler, A. U. Bielinska, K. Janczak, I. Lee, J. R. Baker, *Biochem. Biophys. Res. Commun.* **2001**, *283*, 124–129.
[15] M. Saraswathy, G. T. Knight, S. Pilla, R. S. Ashton, S. Gong, *Colloids Surf. B* **2015**, *126*, 590–597.
[16] Z. Luo, L. Yuwen, Y. Han, J. Tian, X. Zhu, L. Weng, L. Wang, *Biosens. Bioelectron.* **2012**, *36*, 179–185.
[17] X. Chen, J. Chen, H. Dong, Q. Yu, S. Zhang, H. Chen, *J. Electroanal. Chem.* **2019**, *848*, 113244.
[18] R. Gowrishankar, M. K. Hahn, R. D. Blakely, *Neurochem. Int.* **2014**, *73*, 42–48.
[19] S. Stets, T. M. Tavares, P. G. Peralta-Zamora, C. A. Pessoa, N. Nagata, *J. Braz. Chem. Soc.* **2013**, *24*, 1198–1205.
[20] A. A. Mahjoub, A. H. Khan, S. A. S. Sulaiman, R. Lajis, C. N. Man, I. A. H. Ali, *Trop. J. Pharm. Res.* **2016**, *15*, 2475–2481.
[21] K. C. M. S. Lima, A. C. F. Santos, R. N. Fernandes, F. S. Damos, R. C. S. Luz, *Microchem. J.* **2016**, *128*, 226–234.
[22] P. Kanyong, S. Rawlinson, J. Davis, *Chemosensors.* **2016**, *4*, 25–37.
[23] D. R. Carmo, D. S. Fernandes, *Solid State Sci.* **2017**, *71*, 33–41.
[24] N. Laube, B. Mohr, A. Hesse, *J. Cryst. Growth.* **2001**, *233*, 67–74.
[25] S. Stoll, A. Schweiger, *J. Magn. Reson.* **2006**, *178*, 42–55.
[26] A. J. Bard, L. R. Faulkner in, *Electrochemical methods: fundamentals and applications*, *2nd ed.*, John Wiley & Sons, New York, **2001**, pp. 21–26.
[27] Y. Yuan, G. Zhang G, Y. Li, G. Zhang, F. Zhang, X. Fan, *Polym. Chem.* **2013**, *4*, 2164–2167.
[28] Z. Yang, X. Lu, W. Tan, J. Zhao, D. Yang, Y. Yang, Y. He, K. Zhou, *Appl. Surf. Sci.* **2018**, *413*, 1119–1126.
[29] M. Ayiania, M. Smith, A. J. R. Hensley, L. Scudiero, J.-S. McEwen, M. Garcia-Perez, *Carbon* **2020**, *162*, 528–544.
[30] D. A. Beattie, A. Arcifa, I. Delcheva, B. A. Le Cerf, S. V. MacWilliams, A. Rossi, M. Krasowska, *Colloids Surf. A* **2018**, *544*, 78–85.
[31] X. Lin, Q. Xu, L. Gan, G. Owens, Z. Chen, *J. Colloid Interface Sci.* **2022**, *608*, 3159–3167.
[32] J. U. Kiran, J. P. Roners, S. Mathew, *Mater. Today: Proc.* **2020**, *33*, 1263–1267.
[33] N. G. Hădărugă, R. N. Szakal, C. A. Chirilă, A. T. Lukinich-Gruia, V. Păunescu, C. Muntean, G. Rusu, G. Bujancă, D. I. Hădărugă, *Food Chem.* **2019**, *303*, 125419.
[34] N. Devasari, C. P. Dora, C. Singh, S. R. Paidi, V. Kumar, M. E. Sobhia, S. Suresh, *Carbohydr. Polym.* **2015**, *134*, 547–556.
[35] L. F. B. Malaquias, L. C. L. SáBarreto, D. O. Freire, I. C. R. Silva, K. Karan, T. Durig, M. Cunha-Filho, *Carbohydr. Polym.* **2018**, *185*, 19–26.
[36] A. E. Burgos, C. K. Y. A. Okio, R. D. Sinesterra, *Quim. Nova* **2012**, *35*, 762–765.
[37] R. Ebrahimi, B. Hayati, B. Shahmoradi, R. Rezaee, M. Safari, A. Maleki, K. Yetilmezsoy, *Environ. Technol.* **2018**, *12*, 261–272.
[38] D. S. Fernandes, T. F. S. Silveira, U. O. Bicalho, D. R. Do Carmo, *Int. J. Electrochem. Sci.* **2015**, *10*, 2839–2858.
[39] C. W. Ng, J. Ding, Y. Shi, L. M. Gan, *J. Phys. Chem. Solids* **2001**, *62*, 767–775.
[40] M. P. Herring, L. Khachatryan, B. Dellinger, *World Acad. Sci. Eng. Technol.* **2015**, *9*, 804–812.
[41] A. J. Salazar-Medina, R. Sugich-Miranda, E. Teran-Cabanillas, J. Hernández, G. A. González-Aguilar, E. Rudiño-Piñera, R. R. Sotelo-Mundo, E. F. Velázquez-Contreras, *Molecules* **2013**, *18*, 1762–1774.
[42] L. B. Rodrigues, A. O. B. P. B. Martins, J. R. Filho, F. R. A. S. Cesário, F. F. Castro, T. R. Albuquerque, M. N. M. Fernandes, B. A. F. da Silva, L. J. Q. Júnior, A. A. S. Araújo, P. P. Menezes, P. S. Nunes, I. G. Matos, H. D. M. Coutinho, A. G. Wanderley, I. R. A. Menezes, *Food Chem. Toxicol.* **2017**, *109*, 836–846.
[43] G. G. G. Trindade, G. Thrivikraman, P. P. Menezes, C. M. França, B. S. Lima, Y. M. B. G. Carvalho, E. P. B. S. S.

Souza, M. C. Duarte, S. Shanmugam, L. J. Quintans-Júnior, D. P. Bezerra, L. E. Bertassoni, A. A. S. Araújo, *Food Chem. Toxicol.* **2019**, *125*, 198–209.
[44] I. González-Méndez, A. Hameau, R. Laurent, C. Bijani, V. Bourdon, A.-M. Caminade, E. Rivera, K. I. M.-C. Ching, *Eur. J. Org. Chem.* **2020**, *9*, 1114–1121.
[45] M. S. Magossi, V. A. Maraldi, M. S. Magossi, N. L. D. Filho, D. R. Do Carmo, *Electroanalysis* **2018**, *30*, 1–9.
[46] T. F. S. Silveira, M. S. Magossi, M. S. Magossi, U. O. Bicalho, D. R. Do Carmo, *International Journal of Chemistry.* **2014**, *6*, 34–47.
[47] D. Engel, E. W. Grabner, *Ber. Bunsenges. Phys. Chem.* **1985**, *89*, 982–986.
[48] A. P. Baioni, M. Vidotti, P. A. Fiorito, S. I. C. Torresi, *J. Electroanal. Chem.* **2008**, *622*, 219–224.
[49] D. R. Do Carmo, T. R. Souza, V. A. Maraldi, T. F. S. Da Silveira, *Electrocatalysis* **2018**, *9*, 706–715.
[50] D. R. Do Carmo, R. M. D. Silva, N. R. Stradiotto, *Eclética Química J.* **2002**, *27*, 197–210.
[51] D. C. Poudyal, A. K. Satpati, S. Kumar, S. K. Haram, *Mater. Sci. Eng. C* **2019**, *103*, 109788.
[52] S. Schindler, T. Bechtold, *J. Electroanal. Chem.* **2019**, *836*, 94–101.
[53] Y. Li, M. Liu, C. Xiang, Q. Xie, S. Yao, *Thin Solid Films* **2006**, *497*, 270–278.
[54] D. R. Do Carmo, P. F. P. Barbosa, L. R. Cumba, *Silicon.* **2019**, *12*, 1111–1123.
[55] D. R. Do Carmo, D. R. Silvestrini, H. S. Barud, N. L. D. Filho, U. O. Bicalho, L. A. Soares, *J. Nanomater.* **2014**, 695954.
[56] J. F. Giarola, K. B. Borges, C. R. T. Tarley, F. M. Oliveira, E. S. Ribeiro, A. C. Pereira, *Arab. J. Chem.* **2017**, *10*, 430–438.
[57] H. C. de Melo, A. P. D. Seleghim, W. L. Polito, O. Fatibello-Filho, I. C. Vieira, *J. Braz. Chem. Soc.* **2007**, *18*, 797–803.
[58] Z. Qiu, T. Yang, R. Gao, G. Jie, W. Hou, *J. Electroanal. Chem.* **2019**, *835*, 123–129.
[59] S. Priyatharshni, M. Divagar, C. Viswanathan, D. Mangalaraj, N. Ponpandian, *J. Electrochem. Soc.* **2016**, *163*, 460–465.
[60] L. G. Bach, D. M. Nguyen, Q. B. Bui, P. H. Ai-Le, H.-T. Nhac-Vu, *Mater. Chem. Phys.* **2019**, *236*, 121814.
[61] R. Ramachandran, X. Leng, C. Zhao, Z.-X. Xu, F. Wang, *App. Mater. Today.* **2020**, *18*, 100477.
[62] B. B. Li, Y. S. Zhou, W. Wu, M. Liu, S. R. Mei, Y. K. Zhou, T. Jing, *Biosens. Bioelectron.* **2015**, *67*, 121–128.
[63] M. Sarno, S. Galvagno, C. Scudieri, P. Iovane, S. Portofino, C. Borriello, C. Cirillo, *J. Phys. Chem. Solids* **2019**, *131*, 213–222.
[64] F. D. Krampa, Y. Aniweh, P. Kanyong, G. A. Awandare, *Arab. J. Chem.* **2018**, *13*, 3218–3225.
[65] P. Kanyong, S. Rawlinson, J. Davis, *Anal. Bioanal. Chem.* **2016**, *11*, 1–9.
[66] D. Kong, Q. Zhuang, Y. Han, L. Xu, Z. Wang, L. Jiang, J. Su, C.-H. Lu, Y. Chi, *Talanta* **2018**, *185*, 203–212.
[67] S. Meenakshi, S. Devi, K. Pandian, R. Devendiran, M. Selvaraj, *Mater. Sci. Eng. C* **2016**, *69*, 85–94.
[68] E. Nagles, L. Ibarra, J. P. Llanos, J. Hurtado, O. Garcia-Beltrán, *J. Electroanal. Chem.* **2017**, *788*, 38–43.
[69] W. Ji, D. Wu, W. Tang, X. Xi, Y. Su, X. Guo, R. Liu, *Sens. Actuators B* **2019**, *304*, 127414.
[70] T. K. Aparna, R. Sivasubramanian, *Mater. Chem. Phys.* **2019**, *233*, 319–328.

Received: November 12, 2021
Accepted: May 13, 2022
Published online on May 27, 2022

